Discovery of Diagnostic and Therapeutic Targets For Vascular Injury Induced By Methylglyoxal Using Proteomics

Ming-Zhang Xie
Xinxiang Medical University First Affiliated Hospital
Yan-Ting Liu
Xinxiang Medical University First Affiliated Hospital
Min Zhang
Xinxiang Medical University First Affiliated Hospital
Meng-Meng Zhao
Xinxiang Medical University First Affiliated Hospital
Ke-Tao Sun
Zibo Central Hospital
Yu-Chao Zhang
Xinxiang Medical University First Affiliated Hospital
Yu-Jing Zhang
Xinxiang Medical University First Affiliated Hospital
Xiao-Chun Zhou
Xinxiang Medical University First Affiliated Hospital
Lei Wang
Xinxiang Medical University First Affiliated Hospital
De-Ying Bo
Xinxiang Medical University First Affiliated Hospital
Shi-Yan Wang
Xinxiang Medical University First Affiliated Hospital
Guo-An Zhao (tougao3@sohu.com)
Xinxiang Medical University First Affiliated Hospital
Yan-Xuan Liu
Xinxiang Medical University First Affiliated Hospital

Original investigation

Keywords: Human aortic endothelial cells, Laboratory indexes, Methylglyoxal, TMT-based proteomics analysis, Vascular injury

Posted Date: May 20th, 2021

DOI: https://doi.org/10.21203/rs.3.rs-453632/v1

Abstract

Background: Methylglyoxal, a byproduct of diabetes or the consumption of a high-carbohydrate diet, is associated with vascular injury; however, its molecular mechanisms remain unclear. We aimed to systematically characterize molecular profiles and offer unique insights into new disease pathways, thereby contributing to understanding the mechanisms and pathogenesis of vascular injury-related cardiovascular diseases.

Methods: Cell survival assays were performed to assess DNA damage; oxidative stress was confirmed by colorimetric assays and quantitative fluorescence, and cyclooxygenase-2 and the mitogen-activated protein kinase pathways were assessed using ELISA. Differentially expressed proteins were quantitated via TMT-based LC-MS/MS and bioinformatics analysis, and confirmed by parallel reaction monitoring.

Results: Vascular injury was assessed through colorimetric assays, quantitative fluorescence, ELISA, and survival assays. Of the 4029 proteins identified, 368 were differentially expressed after methylglyoxal treatment, compared with the negative control; 31 were defined as biomarkers or therapeutic targets according to the Gene Ontology Program, Kyoto Encyclopedia of Genes and Genomes, and protein-protein interaction network analyses. Sixteen proteins were significantly ($p<0.05$) upregulated (>1.5-fold change) and 15 were dramatically downregulated (<0.667-fold change) and confirmed through parallel reaction monitoring.

Conclusions: The 31 proteins identified as biomarkers or therapeutic targets may contribute to vascular dysfunction through DNA damage, oxidative stress, inflammation, autophagy, hypertension, endothelial dysfunction, vascular remodeling, and the coagulation cascade. Additionally, new disease pathways involving the Wnt, ErBb, and BMP signaling pathways were identified; all provide scope as potential underlying molecular mechanisms. Therefore, the 31 proteins identified warrant further development as new therapeutic or diagnostic targets for vascular diseases.

Highlights

- This study offers three new signaling pathways for VI induced by MGX.
- We classified biomarkers or therapeutic targets for MGX injuries.
- These finding are especially relevant in diabetic patients.

1. Introduction

In humans, methylglyoxal (MGX) is mainly produced in response to a high dietary glycemic load, inducing alterations in glucose and lipid metabolism [1, 2]. The progression of certain diseases—such as vascular injury (VI)—is related to MGX, particularly in people with diabetes, or following consumption of a high-carbohydrate diet [2, 3]. Vascular injuries (VIs) are the leading cause of human death [4], and although the mechanism of how MGX induces VI has still not been elucidated, the key risk in their development was

proven to be endothelial damage. This often includes dynamic changes in a vast collection of molecular events, such as biological processes involving the genome [5, 6], proteome [7, 8], and metabolome [3, 9].

Proteins bear the burden of all biological processes. Simultaneous measurement of a large number of proteins is complicated due to the strong intensity of labor, higher costs, and difficulty of interpreting the bulky results. More recently, these limitations have been overcome by tandem mass tag (TMT)-based liquid chromatography-tandem mass spectrometry (LC-MS/MS) analysis [10]. Therefore, the aim of this study was to systematically characterize these molecular profiles and offer unique insights into disease pathways to promote our understanding of the mechanisms and pathogenesis of VI using TMT-based LC-MS/MS and bioinformatics analysis.

2. Materials And Methods

2.1 Materials

MGX (40% v/v) was purchased from Xiya Chemicals Co., Ltd. (Shandong, China) and dissolved in MilliQ water before use. Human aortic endothelial cells (HAECs) were obtained from Bena Culture Collection Co. (Beijing, China). Fanconi anemia complementation group A (FANCA) siRNA and siRNA-mate were purchased from GenePharma Co., Ltd. (Shanghai, China). Glutathione (GSH) peroxidase assay kits were purchased from the Nanjing Jiancheng Bioengineering Institute (Jiangsu, China). Phospho-extracellular signal-regulated kinase (P-ERK), phospho-c-Jun N-terminal kinase (P-JNK), phospho-p38 kinase (P-P38), and cyclooxygenase-2 (COX-2) ELISA kits were purchased from Abcam (Cambridge, UK), and mitochondrial membrane potential kits were purchased from Abbkine Scientific Co., Ltd. (California, USA); fetal bovine serum (FBS) was obtained from Tianhang (Zhejiang, China).

2.2 siRNA Knockdown of FANCA

HAECs were cultured in Dulbecco's modified Eagle's medium with 10% inactivated FBS in a 5% CO_2 atmosphere at 37°C; to repress FANCA gene expression, siRNA-liposome complexes were formed by mixing FANCA siRNA and siRNA-mate for 10 min at room temperature. HAECs were subsequently incubated for 48–96 h in Dulbecco's modified Eagle's medium with 10% inactivated FBS at 37°C in a 5% CO_2 atmosphere.

2.3 Survival Assays

For the survival assays, HAECs were cultured as described in Sect. 2.2. After 9–12 h, the cells were plated with fresh medium containing a range of indicated concentrations of MGX (0, 5, 10, 15, and 20 μM) daily. Cells were corrected for the concentration of MGX every 24 h and incubated for 8 days to form colonies. The HAECs were rinsed twice with PBS after treatment, and only colonies with more than 50 cells were counted. Drug lethal dose (LD_{50}) values—determined based on the MGX dose producing 50% cell damage—were obtained from the survival curves.

2.4 Measurement of GSH Levels

We analyzed the changes in the intracellular GSH level to confirm oxidative stress. GSH was measured using a GSH detection kit immediately after treatment with MGX (LD_{50}, 10 μM); untreated cells were used as the negative control group. HAECs (1×10^6) were briefly lysed via ultrasound after treatment, mixed with both GSH (1 mM) and reagent 1 (according to the manufacturer's instructions), and incubated at 37°C for 5 min. The results were measured using an absorbance microplate reader (420 nm; Molecular Devices, California, USA) after adding a reaction mixture of reagents 2–5 to the samples and incubating at 37°C for 15 min.

2.5 Measurement of the Mitochondrial Membrane Potential

HAECs were treated with MGX (LD_{50}, 10 μM) or without MGX (control), and the effect of MGX on mitochondrial function was determined using a mitochondrial membrane potential assay kit. Cells were briefly washed and seeded onto a 96-well plate with 100 μl buffer/well. A working solution of the carbocyanine dye JC-1 (100 μl/well) was added after treatment, followed by incubation in the dark at 37°C for 10 min. The results were detected using an F-2500 fluorescence spectrophotometer (Hitachi High-Technologies Corporation, Tokyo, Japan) at λ ex = 529 nm and λ em = 590 nm.

2.6 Measurement of Mitogen-Activated Protein Kinase (MAPK) Pathways and COX-2 using Cell ELISA

To determine the effect of MGX, we assessed the changes in MAPK and COX-2 levels using a cell ELISA kit. First, 100 μL of 10,000 cells were seeded into each well and incubated overnight. HAECs were treated with MGX (LD_{50}, 10 μM), and untreated cells were used as negative controls. Cells were washed and fixed with 100 μL of fixing solution and incubated at room temperature for 20 min. Next, quenching buffer (200 μL) was added for 20 min and washed; the blocking buffer (200 μL) was then added, and the cells were incubated at 37°C for 1 h.Third, primary antibodies (ab126425, ab176660, ab176645, ab267646) were added to corresponding wells, while HRP-conjugated secondary antibodies were incubated at room temperature for 2 h and 1 h, respectively. Finally, they were washed; 100 μL of 3,3',5,5'-tetramethylbenzidine was then incubated and shaken at room temperature for 30 min under light protection; stop solution (50 μl) was then added, and the $OD_{450\ nm}$ of each well was immediately read.

2.7 TMT-Based Proteomics Analysis

2.7.1 Protein Preparation and TMT Labelling

HAECs were treated either with MGX (LD_{50}, 10 μM) or without MGX (control). The lysed HAECs samples were obtained at 70 Hz for 120 s, and the supernatant was collected after centrifugation. Protein digestion was performed according to the FASP procedure described by Wisniewski et al. [11]. The samples were labeled as 126, 127N, 127C, 128N, 128C, 129N, 129C, 130N, 130C, 133C, 133N, and 134N and were multiplexed and vacuum dried.

2.7.2 Peptide Fractionation with Strong Cation Exchange Chromatography

Strong cation exchange chromatography was briefly performed using the AKTA Purifier system (GE Healthcare, Illinois, USA). Gradient elution involving 0–10%, 10–20%, 20–45%, and 50–100% of buffer B (500 mM KCl and 10 mM $KH2PO_4$ in 25% acetonitrile, pH 2.7) was used to elute the peptides at a flow rate of 1 ml/min for 2, 25, 5, and 5 min, respectively; peptides were collected according to the manufacturer's instructions. All fractions were pooled and desalted with C18 standard density cartridges (Empore SPE, 7 mm/3 mL; Sigma-Aldrich, Missouri, USA), vacuum centrifugation, and reconstituted peptides with trifluoroacetic acid.

2.7.3 Liquid chromatography (LC) - electrospray ionization MS/MS analysis using a fusion orbitrap

Briefly, 5 µl of each fraction was analyzed using the Q Exactive HF-X Orbitrap Mass Spectrometer with the Easy nLC system (Thermo Fisher Scientific, Massachusetts, USA), and precursor ions were selected from the survey scan (300–1800 m/z) to obtain MS data. Predictive automatic gain control was used to identify the target value at a resolution of 70000 at m/z 200.

2.7.4 Sequence Database Searching and Data Analysis

The MASCOT engine (version 2.2; Matrix Science, London, UK), Proteome Discoverer 1.4 (Thermo Fisher Scientific), UniProt mus musculus database (87874 sequences, downloaded at 20202603), and decoy database were used to analyze the samples. Samples were measured according to the following parameters: peptide mass tolerance = 20 ppm; MS/MS tolerance = 0.1 Da; enzyme = trypsin; missed cleavage = 2; fixed modification: carbamidomethyl (C), TMT16 (K), TMT16 (N-term); variable modification: oxidation (M); FDR $\leq$ 0.01.

2.7.5 Bioinformatics

Gene ontology (GO) annotated histograms were determined using the Blast2GO program (https://www.blast2go.com/), while the Kyoto Encyclopedia of Genes and Genomes (KEGG) database was used for protein pathway analysis according to the KAAS program (http://www.genome.jp/kaas-bin/kaas_main). Protein-protein interaction (PPI) networks were analyzed using the publicly available program STRING (http://string-db.org/); the minimum required interaction score was set to 0.400. Four sources—genomic context, high-throughput experiments, coexpression, and previous knowledge—were used for direct or indirect PPIs according to STRING.

2.8 Parallel Reaction Monitoring (PRM)

PRM analysis was used to verify different protein expression levels. The TMT protocol (*2.4.1 Protein Preparation and TMT Labeling*) was briefly used to prepare the target peptide, and a standard internal reference was prepared using the stable isotope AQUA peptide. Next, 5–35% acetonitrile gradients were used to perform liquid chromatography for 45 min; Q Exactive Plus MS was used for PRM analysis. The energy of collision, state of charge, and retention time of the target peptides were processed using an optimized protocol. Raw data were subsequently analyzed using Skyline (MacCoss Lab, Seattle, USA), and protein expression levels were determined and compared with those of the control.

2.9 Statistical Analysis

The MS data were analyzed using MaxQuant software version 1.6.5.0 (http://maxquant.org/). Functional annotations were performed by Database for Annotation, and PPI analysis was performed using the STRING database (https://string-db.org/). Data are presented as the mean ± standard deviation from the results of three to five repetitions. The Student's t-test was used to evaluate the statistical differences for paired data, and statistical analyses were performed using SPSS software (version 22.0, SPSS Inc., Illinois, USA); $p < 0.05$ was considered statistically significant.

3. Results

3.1 MGX Partially Inactivates HAECs by DNA Damage, Disrupting GSH, and Depleting the Mitochondrial Membrane Potential, MAP kinase pathways, and Cyclooxygenase-2 (COX-2) Expression

HAECs were treated with either MGX (LD50, 10 μM) or without (control) to detect its effect on the DNA damage, disruption of GSH, and depletion of the mitochondrial membrane potential, MAPK pathways, and COX-2 expression.. To determine whether MGX induced DNA interstrand crosslinks in HAECs, cells were exposed to MGX in the culture medium. HAECs deficient in the FANC pathway (LD_{50} = 9 μM) were moderately sensitive to MGX, compared with HAECs confirmed to be positive for the FANC pathway (LD_{50} = 10 μM; Fig. 1A); therefore, we established DNA damage to be one of the mechanisms of VI; MGX treatment (LD50,10 μM) was performed to determine the level of GSH (62% relative to the negative control group; Fig. 1B) and depletion of mitochondrial membrane potential (46% relative to the negative control group; Fig. 1C). Our results show that oxidative stress occurs in the presence of MGX, thus contributing to the cytotoxicity of HAECs. The COX-2 activation levels increased immediately after MGX treatment (Fig. 1D). The activation levels of the MAPK pathway members, including P-ERK (185%), P-JNK (298%), and P-P38 (157%), increased immediately after MGX treatment (Fig. 1E), thus contributing to the vascular remodeling, disintegrity and dysfunction of HAECs and autophagy.

3.1 Quantitative Proteomic Analysis of HAECs

A total of 4029 potential proteins were identified by LC-MS/MS in HAECs after MGX treatment (LD_{50}, 10 μM) when compared with the negative control; 369 differentially expressed proteins were identified (Supplementary Table 1), of which 228 were upregulated and 141 were downregulated. Statistical analysis (p-value < 0.05) and fold change (FC) cutoff values (FC > 1.5, or < 0.667) referred to the quantitative protein concentration ratios between the MGX treatment and negative control groups. Cluster analysis showed that the protein expression pattern in the treatment group was significantly different from that in the negative control group (Fig. 2).

3.2 Differentially Expressed Proteins Analyzed through KEGG Pathway Annotation and Enrichment

KEGG pathway enrichment analysis was used to determine the functions of the 369 differentially expressed proteins. The top 10 annotated KEGG pathways are shown in Fig. 3. Genetic information processing (e.g., ribosomes, and DNA damage and repair, such as nucleotide excision repair, protein processing in the endoplasmic reticulum, and ubiquitin-mediated proteolysis) was most significantly affected, followed by metabolism (e.g., biosynthesis of unsaturated fatty acids). KEGG pathway annotation analysis indicated that proteins significantly different from those identified during MGX treatment (LD_{50}, 10 μM) correlated with biological functions including DNA damage and repair, oxidative stress, abnormal lipid metabolism, signaling (such as MAPK) pathways, thyroid hormone signaling pathways, autophagy, immune and platelet activation, and so on. More importantly, we formulated unique insights into new disease pathways involving the Wnt, ErBb, and BMP signaling pathways (Supplementary Table 2).

.

3.3 GO Annotation Enrichment Analysis

GO analysis includes three different aspects: cellular components, molecular function, and biological processes. Among the biological processes, the term “biological process” forms the highest percentage, followed by the term “regulation of biological process” (Fig. 4A). Cellular component GO analysis revealed that the terms “intracellular part” and “cytoplasm” were the most crucial factors (Fig. 4B). Accordingly, protein function indicated that protein, RNA, receptor, or enzyme binding were highly enriched, suggesting that MGX has a strong influence on molecular function classification (Fig. 4C). All biological behaviors coordinate with each other and depend on different proteins; thus, we manually analyzed every record in Supplementary Table 1 and classified every differentially expressed protein to further understand the potential underlying molecular mechanisms and offer potential biomarkers or therapeutic targets (Table 1).

Table 1

Classification of each differentially expressed protein according to the GO analysis

GO analysis	Protein group accessions of different proteins (FC > 1.5 or < 0.667)
DNA damage and repair	**A0A087WTQ7 (11)**, A0A0G2JL47, A0A0U1RR8, A0A286YFD6, **A0A2R8Y7V5 (31)**, A0A2R8YD35, **A8K3S0 (2)**, A8K564, B4DET6 (1), **B4DFL3 (7)**, B4DMM2, **B4DWZ4 (12)**, B7Z4H0, **E9PPA5 (24)**, **F5H198 (13)**, H0UI63, **K7ENJ0 (11)**, **M4VP52 (2)**, **P16104 (19)**, P50238 (1), **P51116 (4)**, **P62487 (10)**, **P62877 (9)**, **P62987 (5)**, Q5JXB2 (1), Q6IBT1, Q8N7Z5 (1), **Q96ST3 (4)**, W0S4B9
Oxidation-reduction process	A0A024R9Q1 (1), **A0A024RDA6 (4)**, A0A0S2Z630, **A0A169TED2 (4)**, A0A286YFD6, **A0A2R8Y7V5 (31)**, **A0PJI6 (4)**, A1A4W1, A8K005 (1), A8K734, B0QYA2, B2R4M6 (1), B3KRV6, B4DDP1, B4DFV1 (1), B4DGY8, B4DSD0 (1), **B4DWS6 (2)**, B4DYV0, B6HY68, B7Z553, **B7Z6Y5 (6)**, E9PL41, **F8W0V8 (5)**, H0Y3R4, H0Y3Z3, H0YLC3, H0YMT5, **H7C0V9 (18)**, H7C504, **I3L397 (15)**, **K7X1S0 (3)**, O14654 (1), O43818, O94812, **P01034 (10)**, **P04899 (4)**, **P09211 (2)**, P26022 (1), **P62877 (9)**, **P62987 (5)**, Q15651 (1)(1), Q53H82, Q59EE5 (1), **Q5RLJ0 (2)**, Q68DP2, **Q69EZ8 (9)**, Q969G5, **Q96ST3 (4)**, Q9NQY2, Q9NSI2, V9HW35, W0S4B9
Mitochondrial	**A0A024RDQ7 (6)**, **B2R6X6 (3)**, **B4DFG6 (5)**, B4DL14, B4DXU3, B7Z2L0, B7Z4H0, D6REA0 (1), G3V274, H3BRE2 (1), **H7C0V9 (18)**, H7C2W5 (1), M0QYC4, **P15954 (6)**, P61981, Q3T7B4, Q69YJ6 (1), Q6IBT1, Q8N730, Q8N7F7, **Q8TCC3 (5)**, Q8WVX3, Q9BTT5 (1), **Q9H5Q4 (3)**, **Q9Y399 (10)**
MAPK cascade	**A0A024R2W4 (4)**, A0A024R9Q1 (1), A0A0G2JL47, **A0A169TED2 (4)**, B4DFV1 (1), B4DGY8, B4DIH5, **E7EX60 (2)**, **E9PJK1 (4)**, F8WCI5, H0Y3A3, **H7C0V9 (18)**, O00175, O43818, O94907, P01583 (1), **P04899 (4)**, **P09211 (2)**, **P40306 (7)**, **P62877 (9)**, **P62987 (5)**, **Q5RLJ0 (2)**, Q6IBT1, Q8WVX3, Q969G5, Q96BK8, W0S4B9, **X6RFL8 (5)**
Arterial dysfunction	A0A0S2Z630, A7XZE4, **B7Z6Y5 (6)**, **B7Z8Y6 (5)**, **H7BY41 (2)**, L8ECF6, O00168, **P04899 (4)**, **P09211 (2)**, Q8N1H6, Q8N9J2, Q8NGB0
Vascular remodeling	**A0A024R2W4 (4)**, A0A024R9Q1 (1), A0A0J9YXB6, A0A0S2Z3I2 (1), **A0A0S2Z3U4 (6)**, A0A0S2Z5V0, A0A0S2Z630, A0A0U1RR8, **A0A169TED2 (4)**, **A0A2R8Y7V5 (31)**, A7XZE4, A8K734, B2R4M6 (1), B2R4M6 (1), **B3KM90 (2)**, B3KQD4, B3KRV6, B4DE67 (1), B4DET6 (1), B4DF10, **B4DFL3 (7)**, B4DFV1 (1), B4DIH5, B4DSD0 (1), **B4DTA6 (2)**, **B4DYQ3 (4)**, **B4E0F1 (2)**, B4E1Z9, B7Z553, **B7Z6Y5 (6)**, **B7Z8Y6 (5)**, C9IZY8, C9JG32, **E1A689 (17)**, **E7ETT9 (2)**, **E7EX60 (2)**, E9PL41, F5GY03, F8W9E5, G3V1D0, H0Y3A3, **H3BQ10 (6)**, H3BRE2 (1), H3BSG1, H3BUZ5 (1), **H7C0R2 (6)**, J3KTP9, L8ECF6, **O43237 (5)**, O43818, O75325, O94907, **P01034 (10)**, P01583 (1), P26022 (1), **P40306 (7)**, P52735, **P63173 (7)**, Q08E75, Q14CN4 (1), Q15582 (1), Q4KMP7, **Q4ZG84 (6)**, Q53RZ3, **Q5D862 (3)**, **Q5RLJ0 (2)**, Q68DP2, Q6NX58, Q7Z4H8, Q8N1H6, Q8N730, **Q8WVM7 (2)**, Q8WVX3, Q96BK8, **Q96ST3 (4)**, **Q9BPX5 (2)**, Q9BT25, Q9NX33, Q9UHF1, W0S4B9, **X6RFL8 (5)**
Disintegrity and dysfunction of HAECs	**A0A024R2W4 (4)**, A0A024R9Q1 (1), **A0A024RDA6 (4)**, **A0A0C4DGS1 (17)**, A0A0S2Z3I2 (1), **A0A169TED2 (4)**, A5D8Z7, B2R4M6 (1), B3KQD4, B3KRV6, B4DFV1 (1), **B4DWS6 (2)**, B4E1Z9, B6HY68, **B7Z6Y5 (6)**, **B7Z8Y6 (5)**, **C9J0E4 (3)**, C9J164, D6RAI4, D6RDA2, **E7EX60 (2)**, **E9PJK1 (4)**, F8VUX3, H0Y8R9, H3BS19, H3BUZ5 (1), H7BXY3, O75325, Q53RZ3, **Q5D862 (3)**, Q6P589, Q8N7E2, Q96N83 (1), Q9NQY2, Q9UHF1, **S4R456 (9)**, W0S4B9

Note: Bold-type represents nodes that connect more than two different nodes; numbers in parentheses represent the number of different nodes connected by the same node.

GO analysis	Protein group accessions of different proteins (FC > 1.5 or < 0.667)
Lipid metabolism	A0A0S2Z3I2 (1), A0A0S2Z630, A0A0U1RR8, A0A0U1RR8, **A0PJI6 (4)**, **A8K905 (13)**, B3KRD0, B3KRV6, B4DDP1, B4DE67 (1), B4DFV1 (1), B4DGY8, B4DRY5, B4DSD0 (1), **B4DWS6 (2)**, **B4DYQ3 (4)**, **B4E0F1 (2)**, B6HY68, **B7Z540 (5)**, H0Y3R4, B7Z553, B9TX15, C9JG32, **E1A689 (17)**, E3T200, **E9PJK1 (4)**, H0UI63, H0Y3Z3, H0YLC3, H3BNH5, H3BPL6, H3BS45 (1), H3BSG1, H3BU74, **H7C0V9 (18)**, H7C276 (1), J3KMW2, L8ECF6, O14654 (1) (1), O94907, P01583 (1), P52735, **Q4ZG84 (6)**, Q59EE5 (1), Q6Y1H2, Q7Z4H8, Q8NGB0, Q8WVX3, **Q96ST3 (4)**, Q9ULZ2, Q9Y305
Immunity	A0A024R9Q1 (1), **A0A0C4DGS1 (17)**, A0A0G2JL47, A0A0U1RR8, **A0A169TED2 (4)**, A0A1B0GWD8 (1), **A0A286MCF6 (4)**, A0A286NGJ7, **A0A2R8Y7V5 (31)**, **A0A2U8KGL5 (3)**, **A0A5C2G070 (6)**, A0A5C2G967, A5D8Z7, **A8MVL9 (4)**, B1Q2B0, B2R4M6 (1), **B3KN51 (6)**, **B3KRB2 (5)**, B3KRD0, B3KRV6, **B3KSL3 (5)**, B3KUF5 (1), B4DDP1, **B4DFB1 (3)**, **B4DFL3 (7)**, B4DFV1 (1), **B4DHE5 (4)**, B4DIH5, B4DII5, B4DRY5, B4DYV0, **B4E0F1 (2)**, B4E1Z9, B6HY68, B7Z4H0, C9J164, **C9J7D1 (6)**, C9JG32, **D3DSR2 (3)**, D6RAI4, **D6RD69 (2)**, D6RDA2, **E9PJK1 (4)**, F5GY03, F8VUX3, **F8W0G4 (7)**, H0Y3A3, H0Y3R4, H0Y432, H0Y8R9, **H0YCG2 (5)**, H0YFA4, H0YLT5 (1), H3BRE2 (1), H3BS19, H7BXY3, J3KMW2, **M4VP52 (2)**, O00175, **O43237 (5)**, O43818, **P01034 (10)**, P01583 (1), **P04899 (4)**, **P19474 (5)**, P26022 (1), **P40306 (7)**, P50238 (1), **P51116 (4)**, P52735, **P62987 (5)**, Q4W5D3 (1), **Q5D862 (3)**, Q68DP2, Q69YJ6 (1), Q6IBT1, Q6P589, Q6YHK3, **Q86U29 (3)**, **Q86YZ3 (3)**, Q8N730, Q8WVX3, Q96BK8, Q96DQ4, Q96N83 (1), Q96RS6 (1), Q9BZQ0, **Q9HCE0 (2)**, Q9NQY2, Q9NRX4, Q9P0J7, **Q9Y399 (10)**, W0S4B9, **X6RFL8 (5)**
Autophagy	A1A4G1, A8K005 (1), **B2R4C9 (2)**, B4DET6 (1), **C9J7D1 (6)**, E9PL78, **E9PPA5 (24)**, H3BRE2 (1), O43818, **P19474 (5)**, Q8N730, **Q9HCE0 (2)**, **Q9Y399 (10)**
Blood coagulation	A0A024R9Q1 (1), A0A0U1RR8, **A0A169TED2 (4)**, A0A286NGJ7, **A0A2U8KGL5 (3)**,B2R4M6 (1), B4DFV1 (1), B4DGK9, **B4E380 (5)**, **B7Z8Y6 (5)**, C9J164, **E1A689 (17)**, **E7EX60 (2)**, G3V1S7 (1), **H0YCG2 (5)**, **H3BQ10 (6)**, **H7C0V9 (18)**, **P04899 (4)**, P52735, Q59EE5 (1), **Q69EZ8 (9)**, Q6YHK3, **Q96ST3 (4)**, Q9ULZ2, W0S4B9
NF-κB signaling pathway	B2R4M6 (1), B3KVU0 (1), B4DIH5, C9JTY3, H0Y3A3, H0Y8R9, **H3BQ10 (6)**, H7BXY3, **H7C0V9 (18)**, **P09211 (2)**, **P19474 (5)**, **P62987 (5)**
Wnt signaling pathway	A0A0G2JL47, B4DIH5, B4DXI2, **B4DYQ3 (4)**, **B4E0F1 (2)**, **F5H198 (13)**, H0Y3A3, **H7C0V9 (18)**, O94907, **P40306 (7)**, **P62877 (9)**, **Q4ZG84 (6)**, **Q5RLJ0 (2)**, Q6IBT1, Q96Q45 (1), W0S4B9
ErBb signaling pathways	**A0A169TED2 (4)**, B4DFV1 (1), D6RDA2, **H3BQ10 (6)**, **H7C0V9 (18)**, O94907, **P62987 (5)**, W0S4B9
BMP signaling pathway	**A0A024R0F6 (2)**, F5GY03, O94907, **Q4ZG84 (6)**, W0S4B9

Note: Bold-type represents nodes that connect more than two different nodes; numbers in parentheses represent the number of different nodes connected by the same node.

3.4 PPI Network for Differentially Expressed Proteins

To further understand the biological functions of the differentially expressed proteins, a PPI network was mapped according to the STRING interaction scores (Fig. 5).

PPIs are essential for all biological behaviors; differentially expressed proteins may have the same or better biological function, and proteins with high connectivity may be biomarkers or therapeutic targets affecting the entire biological system. We manually analyzed the biological function of each differentially expressed protein and counted the number of connected nodes that connect to the same node (Supplementary Table 3 and Table 1). .

3.5 Validation of Proteins by PRM

According to GO annotation enrichment analysis and the number of connected nodes that connect to the same node, we manually classified and arranged some key points as biomarkers or therapeutic targets, we used PRM analysis to confirm the FC^{1} (Table 2).

Table 2
Biomarkers or therapeutic targets of disease pathways

GO analysis	Protein accession	Protein	Gene	Nodes	FC[1]	FC[2]
DNA damage and repair	A0A2R8Y7V5	Fanconi anemia subtype D2 protein	FANC D2	31	0.39	0.27
	E9PPA5	Serine/threonine-protein kinase Chk1	CHEK1	24	0.51	0.58
	P16104	Histone H2AX	H2AX	19	3.06	2.56
	B4DWZ4	Flap endonuclease 1	FEN1	12	1. 95	1.77
Oxidation-reduction process	A0A2R8Y7V5	Fanconi anemia subtype D2 protein	FANC D2	31	0.39	0.27
	P62877	E3 ubiquitin-protein ligase RBX1	RBX1	9	0.52	0.45
	P01034	Cystatin-C	CST3	10	0.42	0.53
Mitochondrial	H7C0V9	ABPP	APP	18	0.53	0.36
	Q9Y399	28S ribosomal protein S2, mitochondrial	MRPS2	10	1.87	2.31
	I3L397	Eukaryotic translation initiation factor 5A	EIF5A	15	1.95	1.79
	H7C2W5	NADH dehydrogenase [ubiquinone] 1 alpha subcomplex subunit 10, mitochondrial	NDUFA10	1	14.99	12.84
MAPK cascade	P62877	E3 ubiquitin-protein ligase RBX1	RBX1	9	0.52	0.45
	P40306	Proteasome subunit beta type-10	PSMB10	7	2.45	3.52
	P62987	Ubiquitin-60S ribosomal protein L40	UBA52	5	5. 17	6.49
Arterial dysfunction	B7Z6Y5	cDNA FLJ58696, highly similar to Endoglin	N/A	6	0.42	0.29
	B7Z8Y6	cDNA FLJ58394, highly similar to Platelet endothelial cell adhesion molecule	N/A	5	0.58	0.43
Vascular remodeling	E1A689	Mutant Apo B 100	N/A	17	0.58	0.41

Note: indicates that this protein occurs more than once; FC1 indicates that determination the FC with TMT-based proteomics analysis; FC2 indicates that validation of FC1 by PRM method.

GO analysis	Protein accession	Protein	Gene	Nodes	FC[1]	FC[2]
	B4DFL3	Proteasome subunit beta type-4	N/A	7	3.15	4.21
	B7Z553	cDNA FLJ51266, highly similar to Vitronectin	N/A	0	0.13	0.22
	Q4ZG84	Uncharacterized protein LRP2	LRP2	6	1.90	2.35
Disintegrity and dysfunction of HAECs	A0A0C4DGS1	Dolichyl-diphosphooligosaccharide–protein glycosyltransferase 48 kDa subunit	DDOST	17	2. 99	2.48
	S4R456	40S ribosomal protein S15	RPS15	9	2.16	2.75
	E9PJK1	Tetraspanin	CD81	4	1.53	1.86
	B1ARF3	Type II inositol 1,4,5-trisphosphate 5-phosphatase	INPP5B	2	9.07	12.37
	B7Z6Y5	cDNA FLJ58696, highly similar to Endoglin	N/A	6	0.42	0.29
	B7Z8Y6	cDNA FLJ58394, highly similar to Platelet endothelial cell adhesion molecule	N/A	5	0.58	0.43
Lipid metabolism	H7C0V9	ABPP	APP	18	0.53	0.36
	A0A2R8Y7V5	Fanconi anemia subtype D2 protein	FANC D2	31	0.39	0.27
Immunity and autophagy	A0A2R8Y7V5	Fanconi anemia subtype D2 protein	FANC D2	31	0.39	0.27
	Q9Y399	28S ribosomal protein S2, mitochondria	MRPS2	10	1.87	2.31
	P01034	Cystatin-C	CST3	10	0.42	0.53
	F8W0G4	Poly(rC)-binding protein 2	PCBP2	7	0.63	0.43
	E9PPA5	Serine/threonine-protein kinase Chk1	CHEK1	24	0.51	0.58
	C9J7D1	Ras-related protein Rab-7a	RAB7A	6	0.45	0.49
	H3BQ10	3-phosphoinositide-dependent protein kinase 1	PDPK1	6	2.67	3.25

Note: indicates that this protein occurs more than once; FC1 indicates that determination the FC with TMT-based proteomics analysis; FC2 indicates that validation of FC1 by PRM method.

GO analysis	Protein accession	Protein	Gene	Nodes	FC[1]	FC[2]
Blood coagulation	H7C0V9	ABPP	APP	18	0.53	0.36
	E1A689	Mutant Apo B 100	N/A	17	0.58	0.41
	B7Z553	cDNA FLJ51266, similar to Vitronectin	N/A	0	0.13	0.22
	Q69EZ8	Prothrombin	N/A	9	0.32	0.43
	B4E380	Histone H3	N/A	5	0.45	0.35
NF-κB signaling pathway	P19474	E3 ubiquitin-protein ligase TRIM21	TRIM21	5	1. 19	1.33
	P62987	Ubiquitin-60S ribosomal protein L40	UBA52	5	5. 17	6.49
Wnt signaling pathway	H7C0V9	ABPP	APP	18	0.53	0.36
	F5H198	Damage-specific DNA-binding protein 1	DDB1	13	0.52	0.46
	P62877	E3 ubiquitin-protein ligase RBX1	RBX1	9	0.52	0.45
	P62987	Ubiquitin-60S ribosomal protein L40	UBA52	5	5. 17	6.49
	P40306	Proteasome subunit beta type-10	PSMB10	7	2.45	3.52
ErBb signaling pathways	H7C0V9	ABPP	APP	18	0.53	0.36
	H3BQ10	3-phosphoinositide-dependent protein kinase 1	PDPK1	6	2.67	3.25
	A0A169TED2	Protein kinase C	PRKCA	4	0.60	0.65
BMP signaling pathways	Q4ZG84	Uncharacterized protein LRP2	LRP2	6	1.90	2.35
	A0A024R0F6	Tripartite motif-containing 33, isoform CRA-a	TRIM33	2	1.78	1.91

Note: indicates that this protein occurs more than once; FC1 indicates that determination the FC with TMT-based proteomics analysis; FC2 indicates that validation of FC1 by PRM method.

4. Discussion

Exogenous MGX is present in foods and is an important pollutant, released into the environment through activities such as smoking [12]; however, high levels of endogenous MGX have been found in the plasma of

diabetic patients as the main dicarbonyls [3]. MGX causes VI through DNA damage (Fig. 1A) [13], oxidative stress and mitochondrial dysfunction (Fig. 1B-C) [8], inflammation (Fig. 1D) [14], autophagy (Fig. 1A-E) [3], and hypertension (Fig. 1A-E) [13]. These markers were measured using, making it difficult to reflect the true complexity of VI based on specific pathophysiological concepts. To date, traditional technology has failed to dramatically promote the development of clinical medicine due to high labor and economic costs; these are essential to measure the large amounts of proteins, as well as analyze the bulky, difficult-to-explain clinical results.

To the best of our knowledge, the current study is the first to employ large-scale proteomics to determine the following information after MGX treatment of HAECs; first, the constructed mechanisms of these important molecular profiles (Table 1), corresponding with VI development in their temporal fashion, are considered fundamental to our understanding of the pathogenesis of VI. Second, it offers unique insights into new disease pathways, including Wnt, ErBb, and BMP signaling pathways, providing further opportunities for the development of new diagnostic and therapeutic ideas (Table 2). Third, biological functions were assessed through proteins; we simultaneously manually classified and arranged a large number of biomarkers or therapeutic targets (Table 2) to improve both treatment and prevention, especially in patients with diabetes. Finally, we determined proteins that were dramatically up- or downregulated as a biomarker or drug target based on either the FC (such as accession numbers H7C2W5 or B7Z553), proteins with high connectivity (such as protein accession number A0A2R8Y7V5), or both the FC and proteins with high connectivity, indicating that all biomarkers or therapeutic targets were medically effective.. For example, compared with the negative control, the ratio of protein accession numbers A0A2R8Y7V5 and E9PPA5 were significantly downregulated; this indicated that they were injured and could not work after MGX treatment, resulting in a better therapeutic effect if the level of injured proteins is increased. A few proteins (Table 2) have been listed as diagnostic biomarkers in other papers such as protein accession number P01034; however, these studies either focused on other diseases (such as acute aortic dissection and not VI), or did not include MGX treatment [15].

Our results showed that the FANC pathway contributes to the attenuation of interstrand crosslinks induced by MGX (Fig. 1A); however, to our knowledge, no studies have identified the key proteins involved in DNA damage (Table 1) as a result of MGX cytotoxicity in HAECs. These include: protein accession number A0A2R8Y7V5, which refers to the Fanconi anemia subtype D2 protein (FANC D2), which interacts with multiple proteins to form complexes that participate in interstrand crosslink DNA repair [16]; serine/threonine-protein kinase Chk1 (protein accession number E9PPA5), which weakens DNA damage signaling on autosomes [17]; protein accession number P16104—referring to histone H2AX—which is related to DNA double-strand breaks and helps to recruit DNA repair factors [18]; and protein accession number B4DWZ4, which refers to FEN1, a lethal, synthetic gene resulting in both BRCA1 and BRCA2 loss-of-function [19]. Compared with the negative control, the ratio of protein accession numbers A0A2R8Y7V5 and E9PPA5 were significantly downregulated, indicating that they were injured after MGX treatment; conversely, upregulation of protein accession numbers P16104 and B4DWZ4 means that they worked to repair DNA damage.

Oxidative stress is a key factor that damages HAECs via MGX. Protein accession number A0A2R8Y7V5 refers to a Fanconi anemia subtype D2 protein (BRCA1 or FANC D_2), which may be used in a potential strategy to inhibit energy metabolism by reprogramming mitochondrial metabolism [20]. The cystatin C protein (protein accession number P01034) can inhibit the NF-κB signaling pathway to reduce oxidative stress [21], while the E3 ubiquitin-protein ligase RBX1 protein (protein accession number P62877)—an essential component of the Cul1-Rbx1-Skp1-F boxSkp2 SCF complex—mediates ubiquitination [22]. All three proteins were downregulated, indicating that oxidative stress dramatically damaged HAECs (Table 2); GSH detection results confirmed this conclusion (Fig. 1B).

In addition to producing ATP, the mitochondria are also related to oxidative stress, since the mitochondrial respiratory chain increases the production of reactive oxygen species. The 28S ribosomal protein S2, mitochondrial (protein accession number: Q9Y399) is a necessary component to maintain the structural and essential function of the mitochondria [23], while the APP gene (protein accession number: H7C0V9) relates to age-associated mitochondrial dysfunction in APP/PS1 transgenic mice [24]. The EIF5A gene (protein accession number: I3L397), as well as polyamines regulates mitochondrial substrate oxidation through hypusination of EIF5A [25]. Characterization of protein accession number H7C2W5 variants in wild and spontaneously hypertensive rats indicated the potential pathogenesis of hypertension [26]. Compared with the negative control, protein accession number H7C0V9 was downregulated, indicating that mitochondria were injured after MGX treatment; this was verified by the detection of depleting mitochondrial membrane potential (Fig. 1C). Upregulation of 28S ribosomal protein S2 and eukaryotic translation initiation factor 5A thus, they work to maintain mitochondrial function..

Additionally, we identified several proteins related to the MAPK pathway and measured the activation of these pathways (Fig. 1E) to confirm their biomarkers or therapeutic targets after MGX treatment. E3 ubiquitin-protein ligase RBX1 (protein accession number: P62877) is important for RING-type E3 ligases [27], whereas protein accession number P40306, a proteasome subunit beta type-10, activates the MAPK pathway, enhancing PI resistance by increasing E3 ubiquitin-protein ligase RBX1 capacity [28]. Additionally, ubiquitin-60S ribosomal protein L40 (protein accession number: P62987) and several associated pathways, including MAPK/ERK, might be involved in the development of diffuse large B cell lymphoma [29]. Compared with the negative control, protein accession number P62877 was significantly downregulated, indicating damage after MGX treatment; conversely, protein accession numbers P40306 and P62987 were upregulated, indicating that they worked to activate the MAPK pathway.

Hypertension was confirmed based on the results of the following two proteins: cDNA FLJ58696, highly similar to endoglin (protein accession number: B7Z6Y5), which can both damage and protect vascular function by up- or downregulating the level of protein accession number B7Z6Y5, respectively [30]; and cDNA FLJ58394 (protein accession number: B7Z8Y6), highly similar to platelet endothelial cell adhesion molecule and an attractive target for treating vascular dysfunction through upregulation due to its low expression level [31].

Vascular remodeling was confirmed since the activation of MAPK pathways, DNA damage, oxidative stress, and arterial dysfunction can directly induce vascular structural changes. Our proteomics results also

indicated new biomarkers or therapeutic targets. Mutant Apo B 100 (protein accession number: E1A689), which is downregulated after MGX treatment, can decrease lipid transporter activity and promote arterial stiffness [32], while upregulation (FC = 3.15) of proteasome subunit beta type-4 (protein accession number: B4DFL3) can promote apoptosis by inhibiting cell proliferation [33]. Additionally, uncharacterized protein LRP2 (protein accession number: Q4ZG84) upregulation (FC = 1.90) can promote underlying cases of brain vascular malformation [34], and the biological function of vitronectin (protein accession number: B7Z553) promoted vascular remodeling, such as cell adhesion, migration, or proliferation [35].

Exposure to MGX induced HAEC integrity and dysfunction, causing lipid—especially low-density lipoprotein—movement to the artery wall by passive filtration across a compromised endothelium of high permeability. We have shown that some related biomarkers or therapeutic targets, such as arterial dysfunctional protein accession numbers B7Z6Y5 and B7Z8Y6, can damage vascular functions [30, 31]. New biomarkers or therapeutic targets include the DDOST gene (protein accession number: A0A0C4DGS1), which restored glycosylation in patients' fibroblasts [36]. Upregulation (FC = 2.16) of 40S ribosomal protein S15 (protein accession number: S4R456) can ameliorate senescence to prevent disintegrity and dysfunction by regulating ribosome biogenesis [37]. Tetraspanin (protein accession number: E9PJK1), which is upregulated (FC = 1.53), can enhance the migration of HAECs and lead to pathological vascular remodeling [38]. Upregulation (FC = 9.07) of protein accession number B1ARF3, a type II inositol 1,4,5-trisphosphate 5-phosphatase, can control cell migration, adhesion, and polarity by influencing various aspects of cytoskeletal organization [39].

Exposure to MGX-induced oxidative stress or mitochondrial dysfunction are important factors related to lipid metabolism; for example, MGX causes low-density lipoproteins to react much more actively to the free radical oxidation of lipids [40]. The Fanconi anemia subtype D2 protein (BRCA1) (protein accession number: A0A2R8Y7V5) may potentially be used to inhibit energy metabolism by reprogramming mitochondrial metabolism [20]; ABPP protein (protein accession number: H7C0V9), and age-associated mitochondrial dysfunction in APP/PS1 transgenic mice [24]. The relationship between VI and dyslipidemia is currently of high interest.

Exposure to MGX induced immunity or autophagy, and was confirmed by upregulating the expression of COX-2 (Fig. 1D) [41]. DNA damage (protein accession numbers: A0A2R8Y7V5 and E9PPA5) and oxidative stress (protein accession numbers: P01034, and Q9Y399) can directly induce cell apoptosis or autophagy and clear waste using inflammatory mechanisms, while poly (rC)-binding protein 2 (protein accession number: F8W0G4) exhibits increased caspase-3 activity under oxidative conditions [42]. Suppressed Ras-related protein Rab-7a (protein accession number: C9J7D1), along with NOTCH4 (inducing transcriptional control of RAB proteins) results in the inhibition of vascular inflammation [43]. Finally, upregulated (FC = 2.67) PDPK1 (protein accession number: H3BQ10) can activate autophagy as a sumoylation-regulated kinase [44].

Hemostasis dysfunction is first caused by disruption of the vascular endothelium injuries due to MGX exposure, as well as the dysregulated vascular responses orchestrated by inflammation, hypoxia, apoptosis, and endothelial damage. Activated factor X with its cofactor (factor V) converts prothrombin (protein

accession number: Q69EZ8) to thrombin [45], while histone H3 (protein accession number: B4E380) activates coagulation and thrombosis, even induces coagulation disorders in some cases [46]. Platelets store large amounts of APP fragments (protein accession number: H7C0V9), promoting intact APP expression on the cell surface [47]; previous studies have shown that the various components of Lp(a) (E1A689) may impact platelet activation and aggregation [48], while vitronectin (protein accession number: B7Z553) biology includes platelet aggregation [35]. All these proteins were downregulated, indicating coagulation dysfunction.

Signaling pathways are important for VI induced by MGX, as previous research has reported that MGX directly activates the NF-κB signaling pathway via the MAPK pathway (protein accession number: P62987; FC = 5.17) [41]. Our study shows that protein accession number P19474 is a biomarker or drug target, as trim21 upregulation (FC = 1.62) can improve keratinocyte inflammation by activating the NF-κB pathway [49]. According to GO analysis and KEGG pathway annotation and enrichment, our study is the first to show that the Wnt, ERBB, and BMP signaling pathways are also important for VI induced by MGX; however, the mechanism by which MGX contributes to the pathogenesis of VI through signaling pathways remains unclear.

Up- or downregulation of the following proteins (Table 2) was closely related to the Wnt signaling pathway, as well as VI induced by MGX. DNA damage-binding protein 1 (protein accession number: F5H198) regulates the intracellular level of Pygopus 2, a chromatin effector in the Wnt/β-catenin signaling pathway [50], while the DDB1-Cul4A-Rbx1 complex (protein accession numbers F5H198 and P62877, respectively) increases sumoylation of nuclear c-Myb, which is degraded in response to Wnt-1 signaling [51]. Wnt signaling is increasingly essential in amyloid precursor protein (APP) processing (protein accession number: H7C0V9) [52], as well as the series of molecular signals initiated by binding of a Wnt protein to a frizzled family receptor through protein accession number P62987 [53]; additionally, proteasome subunit beta type-10 (protein accession number: P40306) can modulate the Wnt signaling pathway in MC3T3-E1 cells [54].

Our results also reveal the close relationship between the ErbB or BMP signaling pathways and changes in proteins following MGX treatment. Alzheimer's disease was found to be related to protein accession number H7C0V9, which regulates development from distinct origins, including ErbB signaling pathways [55]. PDK1 (protein accession number: H3BQ10) can cooperate with ERBB-1 through the EGFR-PI3K-PDK1 pathway, regulating ErbB signaling [56], and PRKCA (protein accession number: A0A169TED2) was shown to be associated with neuroactive ligand-receptor interactions and activation of the ErbB signaling pathway [57]. Similarly, the BMP signaling pathway has never been reported to relate to MGX damage. Estrogen receptor alpha (ER) + cells exposed to estradiol induced immediate LRP2 (protein accession number: Q4ZG84; FC = 1.90) activation [58], and TRIM33 (protein accession number: A0A024R0F6; FC = 1.78) was essential for osteoblast proliferation and differentiation via the BMP pathway [59].

To the best our knowledge, this is the first study to offer three new signaling pathways while simultaneously classifying a large number of biomarkers or therapeutic targets (Table 2) to improve both treatment and prevention of MGX injuries, especially in patients with diabetes. However, this study has several limitations;

first, 31 proteins were defined as biomarkers or therapeutic targets. These were determined using HAECs, never confirmed with clinical samples, but can guide to confirm all targets were medical effectiveness with clinical specimens. Second, although new disease pathways involving the Wnt, ErBb, and BMP signaling pathways were determined, further information such as how they contribute to the pathogenesis of VI remains unclear. Finally, several proteins (Table 2) have been listed as diagnostic biomarkers in other papers such as protein accession number P01034; however, they focused on diseases such as acute aortic dissection, rather than MGX induced VI [15].

Declarations

Acknowledgements

We would like to thank Editage (www.editage.cn) for English language editing.

Conflict of Interest:

The authors have no conflicts of interest to report.

Ethics approval and consent to participate

N/A

Consent for publication

N/A

Data Statement:

The data used to support the findings of this study are available from the corresponding author upon request.

Author Contributions

Yan-Xuan Liu, Ming-Zhang Xie, and Guo-An Zhao conceived and designed the study.

Ming-Zhang Xie, Yan-Ting Liu, Min Zhang, Meng-Meng Zhao, Ke-Tao Sun performed the experiments.

Ming-Zhang Xie and Yan-Ting Liu wrote the paper.

Ming-Zhang Xie, Yan-Ting Liu, Yu-Chao Zhang and Guo-An Zhao reviewed and edited the manuscript.

Ming-Zhang Xie, Guo-An Zhao, Yan-Ting, Liu, Min Zhang, Meng-Meng Zhao, Ke-Tao Sun, Yu-Jing Zhang, Xiao-Chun Zhou, De-Ying Bo, Wang Lei, Shi-Yan ,Wang: (1) made substantial contributions to the conception or design of the work or to the acquisition, analysis, or interpretation of data for the work; (2) participated in drafting the work or revising it critically for important intellectual content; (3) approved the final version of the manuscript; and (4) agreed to be accountable for all aspects of the work in ensuring that

questions related to the accuracy or integrity of any part of the work are appropriately investigated and resolved

Funding:

This study was supported by key scientific and technological research projects of Henan Province Foundation (2018020346), key scientific and technological research projects of Henan Province Foundation (LHGJ20190456), first affiliated hospital of Xinxiang Medical University youth science fund project (QN-2019-B02), technology breakthrough plan of Science and Technology Department of Xinxiang (GG2019037)

References

1. Reyaz A, Alam S, Chandra K, Kohli S, Agarwal S. Methylglyoxal and soluble RAGE in type 2 diabetes mellitus: Association with oxidative stress. Journal of diabetes metabolic disorders. 2020;19(1):515–21.
2. Maasen K, van Greevenbroek MMJ, Scheijen J, van der Kallen CJH, Stehouwer CDA, Schalkwijk CG. High dietary glycemic load is associated with higher concentrations of urinary advanced glycation endproducts: the Cohort on Diabetes and Atherosclerosis Maastricht (CODAM) Study. Am J Clin Nutr. 2019;110(2):358–66.
3. Lee JH, Parveen A, Do MH, Kang MC, Yumnam S, Kim SY. Molecular mechanisms of methylglyoxal-induced aortic endothelial dysfunction in human vascular endothelial cells. Cell death disease. 2020;11(5):403.
4. Virani SS, Alonso A, Aparicio HJ, Benjamin EJ, Bittencourt MS, Callaway CW, Carson AP, Chamberlain AM, Cheng S, Delling FN, et al. Heart Disease and Stroke Statistics-2021 Update: A Report From the American Heart Association. Circulation. 2021;143(8):e254–743.
5. Vilanova B, Fernández D, Casasnovas R, Pomar AM, Alvarez-Idaboy JR, Hernández-Haro N, Grand A, Adrover M, Donoso J, Frau J, et al. Formation mechanism of glyoxal-DNA adduct, a DNA cross-link precursor. Int J Biol Macromol. 2017;98:664–75.
6. Chen HC, Chang YL, Teng YC, Hsiao CF, Lin TS. A Stable Isotope Dilution Nanoflow Liquid Chromatography Tandem Mass Spectrometry Assay for the Simultaneous Detection and Quantification of Glyoxal-Induced DNA Cross-Linked Adducts in Leukocytes from Diabetic Patients. Analytical chemistry. 2017;89(24):13082–8.
7. Hanssen NMJ, Scheijen J, Houben A, van de Waarenburg M, Berendschot T, Webers CAB, Reesink KD, van Greevenbroek MMJ, van der Kallen C, Schaper NC, et al. Fasting and post-oral-glucose-load levels of methylglyoxal are associated with microvascular, but not macrovascular, disease in individuals with and without (pre)diabetes: The Maastricht Study. Diabetes Metab. 2021;47(1):101148.
8. Do MH, Lee JH, Ahn J, Hong MJ, Kim J, Kim SY. **Isosamidin from Peucedanum japonicum Roots Prevents Methylglyoxal-Induced Glucotoxicity in Human Umbilical Vein Endothelial Cells via Suppression of ROS-Mediated Bax/Bcl-2**. *Antioxidants (Basel, Switzerland)* 2020, 9(6).

9. Banerjee S. Glyoxal-induced modification enhances stability of hemoglobin and lowers iron-mediated oxidation reactions of the heme protein: An in vitro study. Int J Biol Macromol. 2018;107(Pt A):494–501.
10. Erdjument-Bromage H, Huang FK, Neubert TA: **Sample Preparation for Relative Quantitation of Proteins Using Tandem Mass Tags** (**TMT**) **and Mass Spectrometry** (**MS**). *Methods in molecular biology (Clifton, NJ)* 2018, **1741**:135–149.
11. Wiśniewski JR, Zougman A, Nagaraj N, Mann M. Universal sample preparation method for proteome analysis. Nature methods. 2009;6(5):359–62.
12. Qiu X, Wang S, Ying Q, Duan L, Xing J, Cao J, Wu D, Li X, Chengzhi X, Yan X, et al. Importance of Wintertime Anthropogenic Glyoxal and Methylglyoxal Emissions in Beijing and Implications for Secondary Organic Aerosol Formation in Megacities. Environ Sci Technol. 2020;54(19):11809–17.
13. Patel DM, Bose M, Cooper ME. **Glucose and Blood Pressure-Dependent Pathways-The Progression of Diabetic Kidney Disease**. *International journal of molecular sciences* 2020, 21(6).
14. de Oliveira MG, de Medeiros ML, Tavares EBG, Mónica FZ, Antunes E. Methylglyoxal, a Reactive Glucose Metabolite, Induces Bladder Overactivity in Addition to Inflammation in Mice. Frontiers in physiology. 2020;11:290.
15. Wang HQ, Yang H, Tang Q, Gong YC, Fu YH, Wan F, Yang B, Guo R, Zhong YL, Zhu JM, et al: **Identification of Vinculin as a Potential Diagnostic Biomarker for Acute Aortic Dissection Using Label-Free Proteomics**. *BioMed research international* 2020, **2020**:7806409.
16. Wu RA, Semlow DR, Kamimae-Lanning AN, Kochenova OV, Chistol G, Hodskinson MR, Amunugama R, Sparks JL, Wang M, Deng L, et al. TRAIP is a master regulator of DNA interstrand crosslink repair. Nature. 2019;567(7747):267–72.
17. Abe H, Alavattam KG, Kato Y, Castrillon DH, Pang Q, Andreassen PR, Namekawa SH. CHEK1 coordinates DNA damage signaling and meiotic progression in the male germline of mice. Human molecular genetics. 2018;27(7):1136–49.
18. Plappert-Helbig U, Libertini S, Frieauff W, Theil D, Martus HJ. Gamma-H2AX immunofluorescence for the detection of tissue-specific genotoxicity in vivo. Environ Mol Mutagen. 2019;60(1):4–16.
19. Mengwasser KE, Adeyemi RO, Leng Y, Choi MY, Clairmont C, D'Andrea AD, Elledge SJ. Genetic Screens Reveal FEN1 and APEX2 as BRCA2 Synthetic Lethal Targets. Molecular cell. 2019;73(5):885–99.e886.
20. Kanakkanthara A, Kurmi K, Ekstrom TL, Hou X, Purfeerst ER, Heinzen EP, Correia C, Huntoon CJ, O'Brien D, Wahner Hendrickson AE, et al. BRCA1 Deficiency Upregulates NNMT, Which Reprograms Metabolism and Sensitizes Ovarian Cancer Cells to Mitochondrial Metabolic Targeting Agents. Cancer research. 2019;79(23):5920–9.
21. Su B, Bu SD, Kong BH, Dai RX, Su Q. Cystatin C alleviates H2O2-induced H9c2 cell injury. Eur Rev Med Pharmacol Sci. 2020;24(11):6360–70.
22. Zheng N, Schulman BA, Song L, Miller JJ, Jeffrey PD, Wang P, Chu C, Koepp DM, Elledge SJ, Pagano M, et al. Structure of the Cul1-Rbx1-Skp1-F boxSkp2 SCF ubiquitin ligase complex. Nature. 2002;416(6882):703–9.

23. Cheong A, Lingutla R, Mager J. Expression analysis of mammalian mitochondrial ribosomal protein genes. Gene Expr Patterns. 2020;38:119147.
24. Chen L, Xu S, Wu T, Shao Y, Luo L, Zhou L, Ou S, Tang H, Huang W, Guo K, et al. Studies on APP metabolism related to age-associated mitochondrial dysfunction in APP/PS1 transgenic mice. Aging. 2019;11(22):10242–51.
25. Bekebrede AF, Keijer J, Gerrits WJJ, Boer VCJ. **The Molecular and Physiological Effects of Protein-Derived Polyamines in the Intestine**. *Nutrients* 2020, 12(1).
26. Huang L, Jin X, Xia L, Wang X, Yu Y, Liu C, Shao D, Fang N, Meng C. Characterization of mitochondrial NADH dehydrogenase 1α subcomplex 10 variants in cardiac muscles from normal Wistar rats and spontaneously hypertensive rats: Implications in the pathogenesis of hypertension. Mol Med Rep. 2016;13(1):961–6.
27. Achiwa Y, Hasegawa K, Udagawa Y. Effect of ursolic acid on MAPK in cyclin D1 signaling and RING-type E3 ligase (SCF E3s) in two endometrial cancer cell lines. Nutrition cancer. 2013;65(7):1026–33.
28. Shirazi F, Jones RJ, Singh RK, Zou J, Kuiatse I, Berkova Z, Wang H, Lee HC, Hong S, Dick L, et al. Activating KRAS, NRAS, and BRAF mutants enhance proteasome capacity and reduce endoplasmic reticulum stress in multiple myeloma. Proc Natl Acad Sci USA. 2020;117(33):20004–14.
29. Nigro C, Leone A, Raciti GA, Longo M, Mirra P, Formisano P, Beguinot F, Miele C. **Methylglyoxal-Glyoxalase 1 Balance: The Root of Vascular Damage**. *International journal of molecular sciences* 2017, 18(1).
30. Leite AR, Borges-Canha M, Cardoso R, Neves JS, Castro-Ferreira R, Leite-Moreira A. Novel Biomarkers for Evaluation of Endothelial Dysfunction. Angiology. 2020;71(5):397–410.
31. Lertkiatmongkol P, Liao D, Mei H, Hu Y, Newman PJ: **Endothelial functions of platelet/endothelial cell adhesion molecule-1 (CD31)**. *Current opinion in hematology* 2016, **23**(3):253–259.
32. Czeck MA, Northrop EF, Evanoff NG, Dengel DR, Rudser KD, Kelly AS, Ryder JR. Relationship of Apolipoproteins with Subclinical Cardiovascular Risk in Youth. J Pediatr. 2020;227:199–203.e191.
33. Cheng YC, Tsai WC, Sung YC, Chang HH, Chen Y. Interference with PSMB4 Expression Exerts an Anti-Tumor Effect by Decreasing the Invasion and Proliferation of Human Glioblastoma Cells. Cellular physiology biochemistry: international journal of experimental cellular physiology biochemistry pharmacology. 2018;45(2):819–31.
34. Zhang M, Ding X, Zhang Q, Liu J, Zhang Y, Zhang Y, Tian Z, Li W, Zhu W, Kang H, et al: **Exome sequencing of 112 trios identifies recessive genetic variants in brain arteriovenous malformations**. *Journal of neurointerventional surgery* 2020.
35. Preissner KT, Reuning U. Vitronectin in vascular context: facets of a multitalented matricellular protein. Semin Thromb Hemost. 2011;37(4):408–24.
36. Jones MA, Ng BG, Bhide S, Chin E, Rhodenizer D, He P, Losfeld ME, He M, Raymond K, Berry G, et al. DDOST mutations identified by whole-exome sequencing are implicated in congenital disorders of glycosylation. Am J Hum Genet. 2012;90(2):363–8.

37. Wu S, Xu S, Li R, Li K, Zhong X, Li Y, Zhou Z, Liu Y, Feng R, Zheng J, et al. mTORC1-Rps15 Axis Contributes to the Mechanisms Underlying Global Translation Reduction During Senescence of Mouse Embryonic Fibroblasts. Frontiers in cell developmental biology. 2019;7:337.
38. Zhang Y, Wang J, Ding Y, Zhang J, Xu Y, Xu J, Zheng S, Yang H. Migrasome and Tetraspanins in Vascular Homeostasis: Concept, Present, and Future. Frontiers in cell developmental biology. 2020;8:438.
39. Ramos AR, Elong Edimo W, Erneux C. Phosphoinositide 5-phosphatase activities control cell motility in glioblastoma: Two phosphoinositides PI(4,5)P2 and PI(3,4)P2 are involved. Advances in biological regulation. 2018;67:40–8.
40. Lankin VZ, Tikhaze AK, Kapel'ko VI, Shepel'kova GS, Shumaev KB, Panasenko OM, Konovalova GG, Belenkov YN. Mechanisms of oxidative modification of low density lipoproteins under conditions of oxidative and carbonyl stress. Biochemistry Biokhimiia. 2007;72(10):1081–90.
41. Lin CC, Chan CM, Huang YP, Hsu SH, Huang CL, Tsai SJ. Methylglyoxal activates NF-κB nuclear translocation and induces COX-2 expression via a p38-dependent pathway in synovial cells. Life sciences. 2016;149:25–33.
42. Ishii T, Igawa T, Hayakawa H, Fujita T, Sekiguchi M, Nakabeppu Y. PCBP1 and PCBP2 both bind heavily oxidized RNA but cause opposing outcomes, suppressing or increasing apoptosis under oxidative conditions. J Biol Chem. 2020;295(34):12247–61.
43. Jin K, Wen Z, Wu B, Zhang H, Qiu J, Wang Y, Warrington KJ, Berry GJ, Goronzy JJ, Weyand CM. **NOTCH-induced rerouting of endosomal trafficking disables regulatory T cells in vasculitis**. *The Journal of clinical investigation* 2021, 131(1).
44. Hu B, Zhang Y, Deng T, Gu J, Liu J, Yang H, Xu Y, Yan Y, Yang F, Zhang H, et al: **PDPK1 regulates autophagosome biogenesis by binding to PIK3C3**. *Autophagy* 2020:1–18.
45. Umerah CO. Momodu, II: **Anticoagulation**. In: *StatPearls.* Treasure Island (FL): StatPearls Publishing Copyright © 2021. StatPearls Publishing LLC.; 2021.
46. Li L, Yu S, Fu S, Ma X, Li X. Unfractionated heparin inhibits histone-mediated coagulation activation and thrombosis in mice. Thrombosis research. 2020;193:122–9.
47. Canobbio I, Catricalà S, Balduini C, Torti M. Calmodulin regulates the non-amyloidogenic metabolism of amyloid precursor protein in platelets. Biochim Biophys Acta. 2011;1813(3):500–6.
48. Discepolo W, Wun T, Berglund L. Lipoprotein(a) and thrombocytes: potential mechanisms underlying cardiovascular risk. Pathophysiol Haemost Thromb. 2006;35(3–4):314–21.
49. Yang L, Zhang T, Zhang C, Xiao C, Bai X, Wang G. Upregulated E3 ligase tripartite motif-containing protein 21 in psoriatic epidermis ubiquitylates nuclear factor-κB p65 subunit and promotes inflammation in keratinocytes. Br J Dermatol. 2021;184(1):111–22.
50. Li Q, Li Y, Gu B, Fang L, Zhou P, Bao S, Huang L, Dai X. Akt Phosphorylates Wnt Coactivator and Chromatin Effector Pygo2 at Serine 48 to Antagonize Its Ubiquitin/Proteasome-mediated Degradation. J Biol Chem. 2015;290(35):21553–67.

51. Kanei-Ishii C, Nomura T, Egoh A, Ishii S. Fbxw5 suppresses nuclear c-Myb activity via DDB1-Cul4-Rbx1 ligase-mediated sumoylation. Biochem Biophys Res Commun. 2012;426(1):59–64.
52. Tapia-Rojas C, Inestrosa NC. Loss of canonical Wnt signaling is involved in the pathogenesis of Alzheimer's disease. Neural regeneration research. 2018;13(10):1705–10.
53. Huelsken J, Birchmeier W. New aspects of Wnt signaling pathways in higher vertebrates. Curr Opin Genet Dev. 2001;11(5):547–53.
54. Schroeder TM, Nair AK, Staggs R, Lamblin AF, Westendorf JJ. Gene profile analysis of osteoblast genes differentially regulated by histone deacetylase inhibitors. BMC Genomics. 2007;8:362.
55. Ma N, Tie C, Yu B, Zhang W, Wan J. Circular RNAs regulate its parental genes transcription in the AD mouse model using two methods of library construction. FASEB journal: official publication of the Federation of American Societies for Experimental Biology. 2020;34(8):10342–56.
56. Xia H, Dai X, Yu H, Zhou S, Fan Z, Wei G, Tang Q, Gong Q, Bi F. EGFR-PI3K-PDK1 pathway regulates YAP signaling in hepatocellular carcinoma: the mechanism and its implications in targeted therapy. Cell death disease. 2018;9(3):269.
57. Xu C, Li R, Wu J. Effects of Yuanhu- Zhitong tablets on alcohol-induced conditioned place preference in mice. Biomedicine pharmacotherapy = Biomedecine pharmacotherapie. 2021;133:110962.
58. Meng P, Vaapil M, Tagmount A, Loguinov A, Vulpe C, Yaswen P. Propagation of functional estrogen receptor positive normal human breast cells in 3D cultures. Breast cancer research treatment. 2019;176(1):131–40.
59. Guo J, Qin W, Xing Q, Gao M, Wei F, Song Z, Chen L, Lin Y, Gao X, Lin Z. TRIM33 is essential for osteoblast proliferation and differentiation via BMP pathway. Journal of cellular physiology. 2017;232(11):3158–69.

Figures

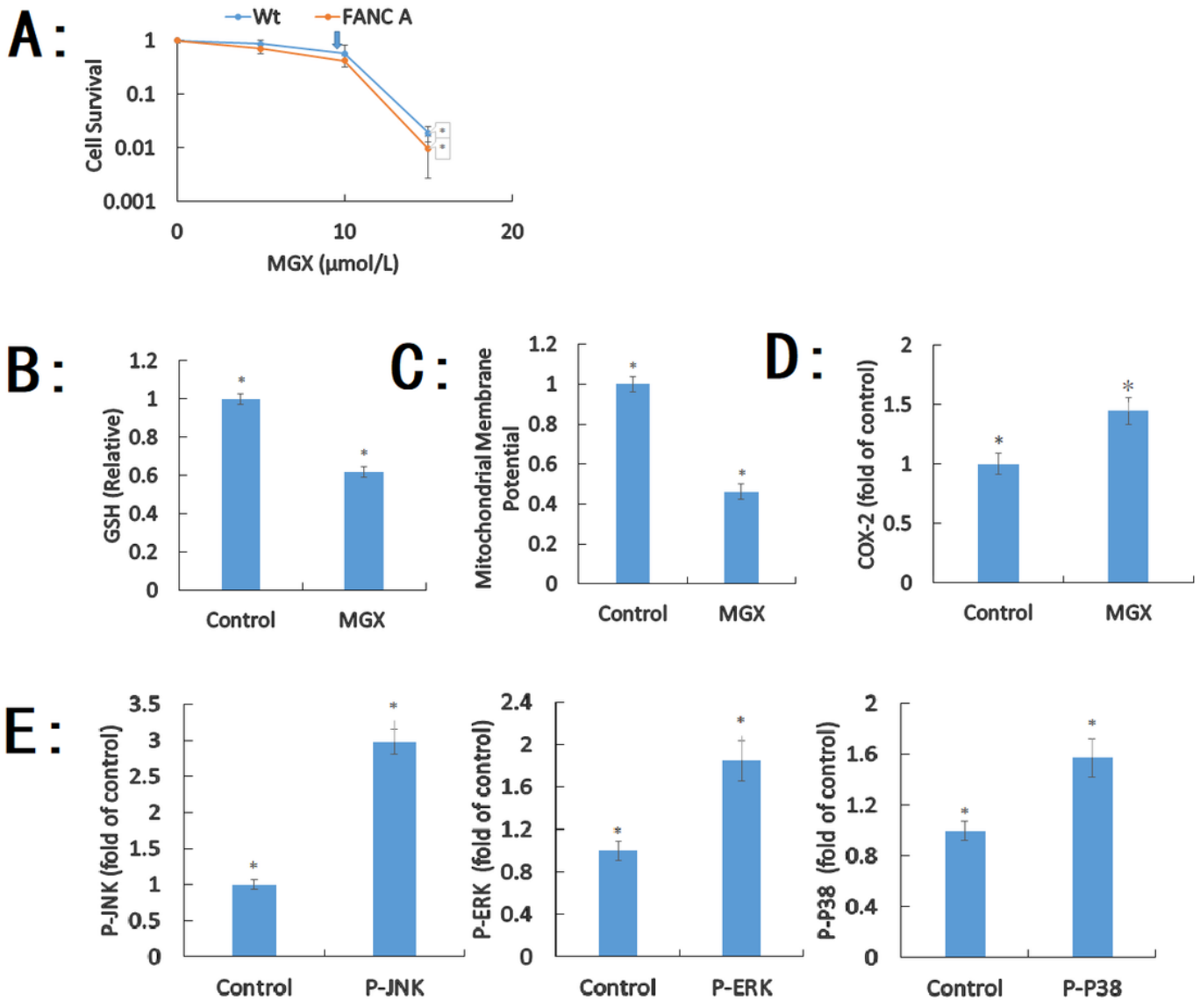

Figure 1

Human aortic endothelial cells (HAECs) treated with methylglyoxal (MGX) to detect its effect on DNA damage, oxidative stress, MAPK pathways, and COX-2 expression (A) Analysis of DNA damage in HAECs deficient in the FANC pathway induced by MGX. HAECs were treated with a range of concentrations (0, 5, 10, 15, and 20 μM) of MGX for 8 days before survival was determined. Drug lethal dose (LD50) values were confirmed from survival curves and are indicated by an arrow. Data are the means with standard deviations of five independent experiments. (B) Effect of MGX on the level of GSH. (C) Effect of MGX on depletion of the mitochondrial membrane potential. (D) COX-2 was activated by MGX. (E) MAPK pathways, including P-ERK, P-JNK, and P-P38, were activated by MGX. Statistically significant differences are indicated by an asterisk; $p<0.05$ indicates statistical significance.

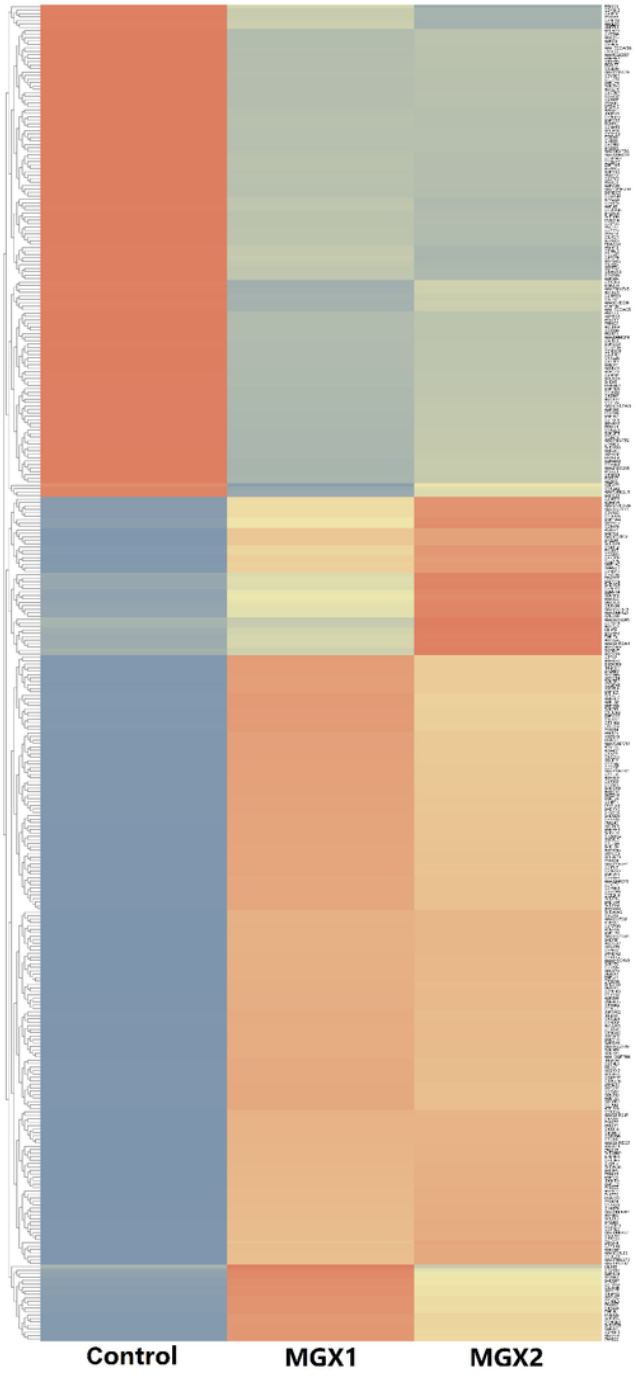

Figure 2

Heatmap of differentially expressed proteins. Each row represents a different protein, whereas columns represent different samples. Each color represents a different quantity of expression (log2 expression). Red indicates the higher levels of proteins and blue indicates lower level proteins.

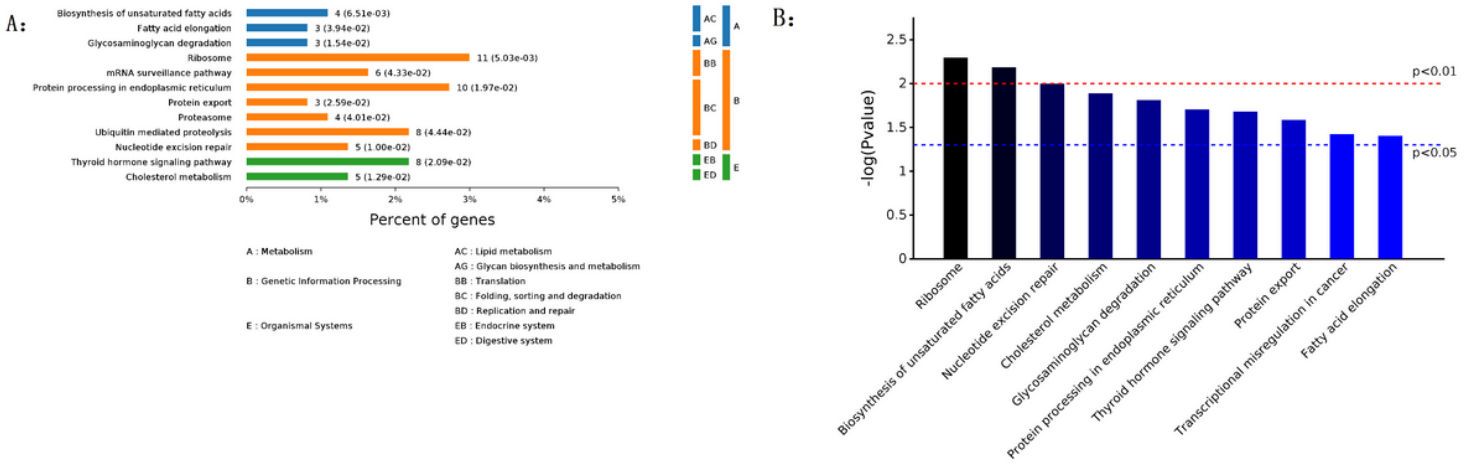

Figure 3

Differentially expressed proteins identified by Kyoto Encyclopedia of Genes and Genomes (KEGG) pathway annotations (A) The abscissa represents the percentage of genes; the ordinate lists the KEGG pathways. (B) The blue line indicates p<0.05, and the red line indicates p<0.01.

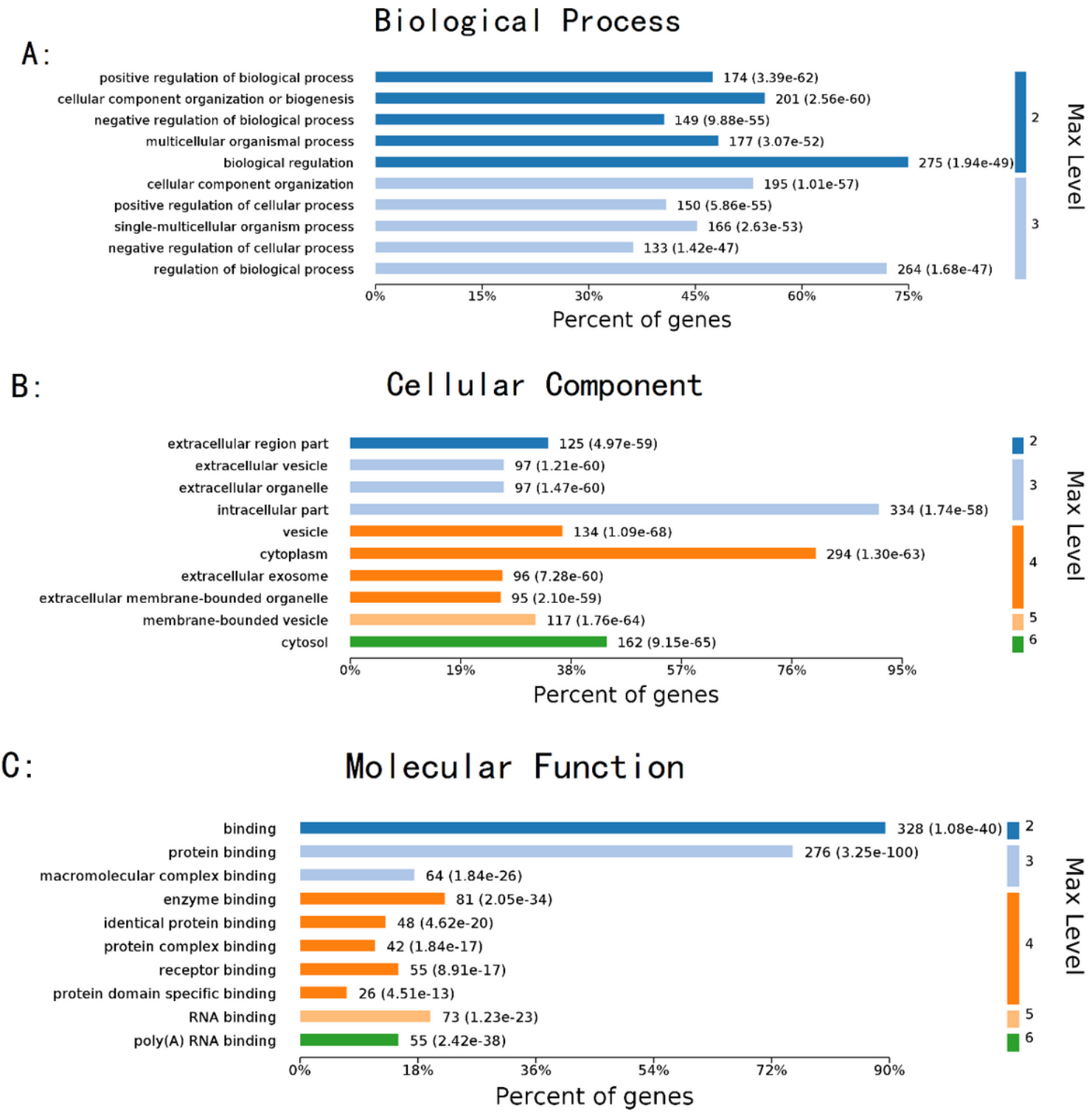

Figure 4

Gene ontology (GO) enrichment for different protein expressions Top 10 biological process (A), molecular function (B), and cellular component (C) enrichment terms. The abscissa represents the percent of genes, while the ordinate indicates the details of enrichment terms ($p<0.01$).

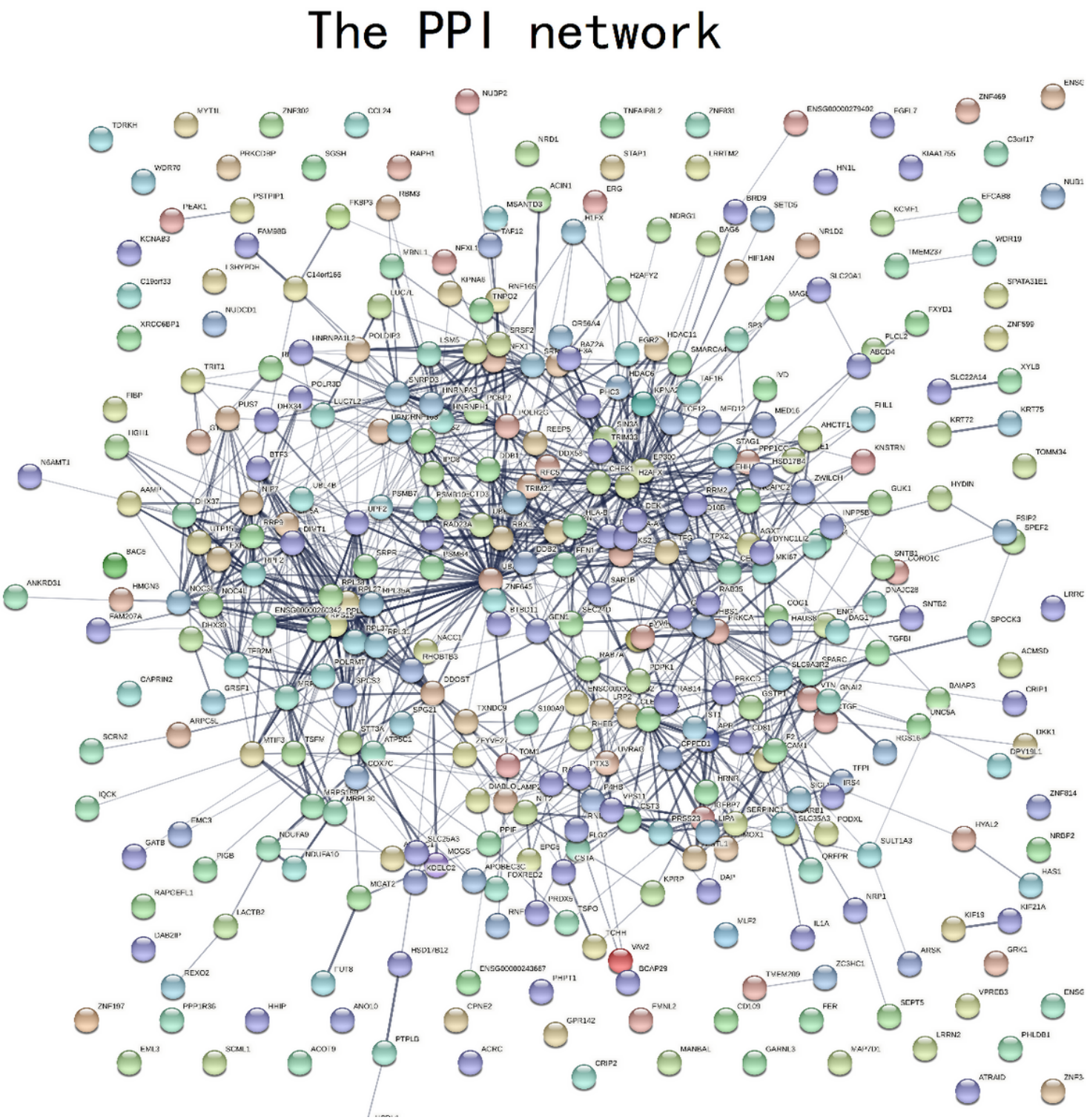

Figure 5

Using the STRING database to determine protein-protein interactions between differentially expressed proteins.Nodes represent the proteins and lines represent protein-protein interactions.